NANO LETTERS
Letter
Cite This: Nano Lett. 2018, 18, 4136−4140
pubs.acs.org/NanoLett

Environmental Electrometry with Luminescent Carbon Nanotubes

Jonathan C. Noé,[†] Manuel Nutz,[†] Jonathan Reschauer,[†] Nicolas Morell,[‡] Ioannis Tsioutsios,[‡] Antoine Reserbat-Plantey,[‡] Kenji Watanabe,[§] Takashi Taniguchi,[§] Adrian Bachtold,[‡] and Alexander Högele*,[†]

[†]Fakultät für Physik, Munich Quantum Center, and Center for NanoScience (CeNS), Ludwig-Maximilians-Universität München, Geschwister-Scholl-Platz 1, 80539 München, Germany

[‡]The Barcelona Institute of Science and Technology, ICFO-Institut de Ciències Fotòniques, The Barcelona Institute of Science and Technology, 08860 Castelldefels, Spain

[§]National Institute for Materials Science, Tsukuba, Ibaraki 305-0044, Japan

Supporting Information

ABSTRACT: We demonstrate that localized excitons in luminescent carbon nanotubes can be utilized to study electrostatic fluctuations in the nanotube environment with sensitivity down to the elementary charge. By monitoring the temporal evolution of the cryogenic photoluminescence from individual carbon nanotubes grown on silicon oxide and hexagonal boron nitride, we characterize the dynamics of charge trap defects for both dielectric supports. We find a one order of magnitude reduction in the photoluminescence spectral wandering for nanotubes on extended atomically flat terraces of hexagonal boron nitride. For nanotubes on hexagonal boron nitride with pronounced spectral fluctuations, our analysis suggests proximity to terrace ridges where charge fluctuators agglomerate to exhibit areal densities exceeding those of silicon oxide. Our results establish carbon nanotubes as sensitive probes of environmental charge fluctuations and highlight their potential for applications in electrometric nanodevices with all-optical readout.

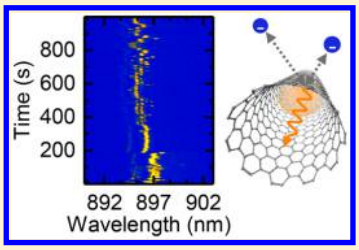

KEYWORDS: *Carbon nanotubes, localized excitons, photoluminescence spectroscopy, environmental electrometry, charge fluctuations, hexagonal boron nitride*

Carbon nanotubes (CNTs) provide sensing capabilities in areas as diverse as optical bioimaging[1,2] or single-molecule,[3] temperature,[4] and strain[5,6] detection. Semiconducting CNTs with diameters of about 1 nm and respective optical transitions in the near-infrared[7,8] combine such sensing functionalities with the convenience of an optical readout.[4−6] Moreover, the permanent electric dipole moment of localized excitons[9,10] adds means of electrostatic environmental sensing to the realm of all-optical reporting capabilities of individual nanotubes, placing them alongside semiconductor quantum dots[11−14] and charged nitrogen vacancy centers in diamond[15,16] as elementary sensing units in all-optical electrometers.

Individual CNTs report changes in electric field via spectral shifts in their photoluminescence (PL) energy. A dynamically fluctuating charge environment results in spectral fluctuations in the course of time which are particularly pronounced for localized excitons exhibiting finite electric dipole moments[9,10] as a consequence of localization at unintentional disorder[17] or at side-wall defects in chemically functionalized nanotubes.[18−21] Consistently, spectral fluctuations are suppressed for excitons in suspended nanotubes sufficiently far away from the fluctuating charge reservoir of dielectric supports.[22,23] Electrostatically passive environments of polymers yield similar trends.[24]

In this work, we utilize the sensitivity of CNT exciton PL to variations in local electric fields to study the dynamics of charge fluctuations in silicon oxide (SiO_2) and hexagonal boron nitride (hBN) supports. While SiO_2 is a standard material in industrial integrated circuitry and is commonly used as dielectric support for prototype devices based on novel materials, the practicability of silicon platforms is challenged by the limitations in device performance due to fluctuating charge impurities inherent to SiO_2. They are known to reduce the intrinsic charge carrier mobility in graphene,[25,26] to cause hysteretic effects in CNT transistors,[27−29] or to limit the sensitivity of nanotube-based biomolecular sensors.[3,30] Recent transport studies of graphene[31−33] and CNTs[34] on hBN on the other hand indicate that such detrimental effects are reduced on atomically flat hBN supports. More recent optical studies of two-dimensional semiconductors have confirmed the beneficial impact of hBN environments by reporting spectral line widths at the limit of homogeneous broadening in best samples with both-sided hBN encapsulation.[35−38]

To probe the charge noise characteristics of SiO_2 and hBN, we performed PL spectroscopy of individual CNTs grown directly on both dielectric supports. The sample was prepared by chemical vapor deposition (CVD), and cryogenic PL studies were performed in a home-built confocal microscope

Received: March 2, 2018
Revised: June 12, 2018
Published: June 19, 2018

DOI: 10.1021/acs.nanolett.8b00871
Nano Lett. 2018, 18, 4136−4140

immersed in a liquid helium bath cryostat with a base temperature of 4.2 K (see Supporting Information for details). Figure 1a shows a map of PL peak intensities recorded in the

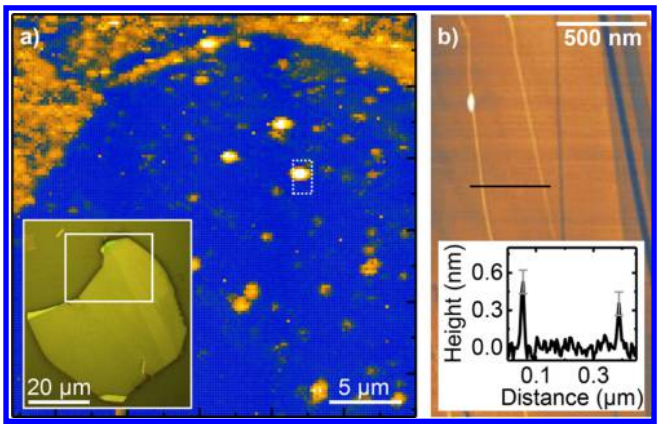

Figure 1. (a) Cryogenic raster-scan photoluminescence map of a region with an ∼300 nm thick hBN flake on SiO_2 indicated by the white rectangle in the optical image inset (different aspect ratios are due to nonlinearities in low-temperature scanning). The contrast between the regions of SiO_2 (orange) and hBN (blue) stems from a much weaker photoluminescence background on hBN. (b) Atomic force micrograph of the area marked by the dashed white rectangle in (a) identifies two carbon nanotubes and hBN crystal terraces. Inset: Height profile of the nanotubes taken along the black line.

region of an hBN flake on SiO_2 (indicated in the optical micrograph inset) at 100 μW excitation power of a circularly polarized laser. The edge of the hBN flake in Figure 1a is identified by a crossover from a dark-count limited background on hBN to a finite PL background on SiO_2. The logarithmic false-color scale of the PL map exaggerates the PL background on SiO_2 with respect to the 1 order of magnitude brighter PL hot spots stemming from individual CNTs with peak intensities of 15−130 cts/s. CVD-grown tubes of five chiralities with emission wavelengths in the range 850−1000 nm, namely (5,4),(6,4),(9,1),(8,3), and (6,5), are expected to dominate the PL in the spectral window of our silicon charge-coupled device. Consistently, CNTs with corresponding diameters below 1 nm were identified on our sample with atomic force microscopy (AFM) both on bare SiO_2 and on hBN (the respective AFM image of two nanotubes on hBN is shown in Figure 1b).

The hot spots of local and intense PL in Figure 1a correspond to individual nanotubes with spectrally narrow PL peaks characterized by resolution-limited full width at half-maximum (fwhm) line widths of ∼200 μeV at short integration times of 1 s (representative spectra are shown in the top and bottom panels of Figure 2a for two different nanotubes on hBN and SiO_2, respectively). In contrast to the narrow PL spectra observed at lowest integration times of 1 s both on hBN and SiO_2, a large fraction of nanotubes lying on SiO_2 developed highly asymmetric spectra with significant spectral broadening at increased integration times (compare the spectra with 1 and 100 s integration times in Figure 2a). This time-accumulated PL line broadening was also observed at the statistical level for different CNTs on hBN and SiO_2; the histogram of Figure 2b with a fwhm binning of 0.5 meV shows that the PL line width of nanotubes on hBN (blue columns) was independent of the integration time, while the spectra of most nanotubes on SiO_2 exhibited a progressively increasing spectral broadening with prolonged integration times.

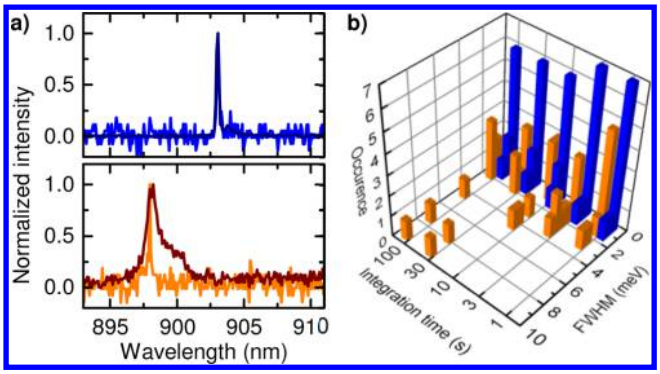

Figure 2. (a) Low-temperature photoluminescence spectra of individual carbon nanotubes on hBN (top panel) and SiO_2 (bottom panel) at 18 μW excitation power. Blue (orange) and dark blue (wine) spectra were recorded with 1 and 100 s integration times, respectively. (b) Histogram of the fwhm line widths of carbon nanotube photoluminescence spectra on SiO_2 (orange) and hBN (blue) as a function of the integration time.

To examine this pronounced difference in the temporal evolutions of the emission from CNTs on hBN and SiO_2 in more detail, we sampled the PL with 1 s integration time over the course of 1000s and color-coded the PL evolution as in Figure 3a. The temporal characteristics of individual CNTs in

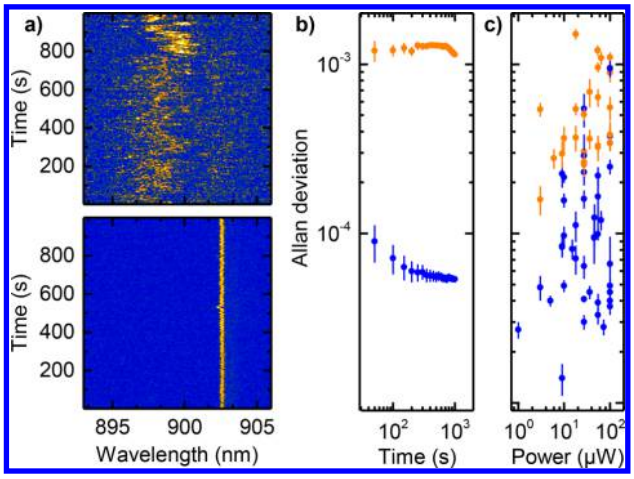

Figure 3. (a) Temporal evolution of the photoluminescence of a representative carbon nanotube on SiO_2 (top) and on hBN (bottom) at 18 μW excitation power. (b) Corresponding temporal evolutions of the Allan deviations. (c) Allan deviations for carbon nanotubes on SiO_2 (orange) and hBN (blue) at different excitation powers calculated from sets of 100 consecutive spectra with 1 s integration time per spectrum.

the upper and lower panels of Figure 3a are representative for substrate-specific responses observed on SiO_2 and hBN, respectively, with frequent spectral fluctuations on millielectronvolt scale for tubes on SiO_2 contrasted by CNTs on hBN with stable PL emission. A quantitative analysis of this effect was performed using the Allan deviation as a measure for the spectral stability of a resonance[39,40] (see Supporting Information). For the two specific CNTs on SiO_2 and hBN of Figure 3a, the Allan deviation calculated in steps of 50 s and displayed in Figure 3b (orange and blue data correspond to the CNT on SiO_2 and hBN, respectively) was found to differ by more than 1 order of magnitude on all time scales of our experiment.

DOI: 10.1021/acs.nanolett.8b00871
Nano Lett. 2018, 18, 4136−4140

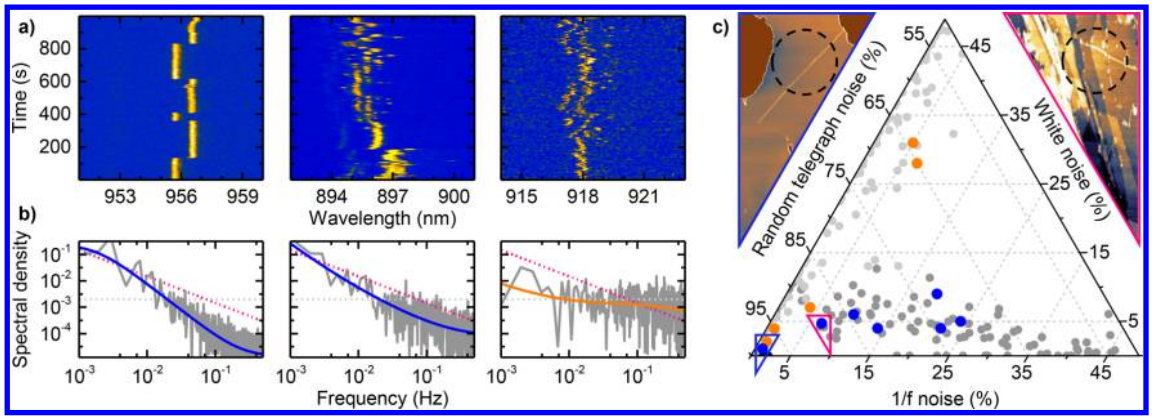

Figure 4. (a) Temporal evolution of carbon nanotube photoluminescence representing the cases of a large random telegraph, $1/f$ and white noise component (from left to right) in their spectral fluctuations at 4.2 K. (b) Respective normalized noise spectral densities and model decompositions (solid lines, orange and blue colors represent nanotubes on SiO_2 and hBN, respectively) into random telegraph, $1/f$ and white noise according to eq 1. The pink and gray dashed lines indicate the limits of pure $1/f$ and white noise, respectively. (c) Noise composition of carbon nanotubes on hBN (blue data points) and on SiO_2 (orange data points). The gray data are simulation results connecting the measurements to physical substrate properties. They represent the expected distribution of fluctuating charge traps on SiO_2 (light gray) contrasted by the scenario of an electrostatically calm substrate with and without accumulation of distant surface states (black and gray, respectively; the black data points are concentrated at the lower left corner of the ternary diagram and are therefore barely distinguishable). Insets: Atomic force micrographs of CNTs on flat and rocky regions of an hBN flake (blue and pink triangles, respectively, also used to indicate the corresponding noise compositions in the ternary plot; the dashed circles mark the optical spot with ~1 μm diameter).

The Allan deviation of 19 different CNTs on SiO_2 and hBN as a function of the excitation laser power is shown in Figure 3c as orange and blue data, respectively. The graph divides the tubes on hBN and SiO_2 into two disparate classes, with a few exceptions of CNTs on hBN exhibiting spectral fluctuations as large as most of the CNTs on SiO_2. The large spread in the data shows no obvious trend for the functional dependence of the PL stability on the excitation power for tubes on hBN, while the spectral fluctuations seem to increase for tubes on SiO_2 with higher excitation powers in accord with power-induced spectral wandering.[41] These observations suggest that spectral fluctuations are sensitive to the specifics of the dielectric support, and that the charge noise in the PL of nanotubes on hBN is strongly inhibited.

To clarify the origin of large spectral wandering for those tubes on hBN that exhibited Allan deviation values comparable to CNTs on SiO_2 in Figure 3c, we analyzed the details of the charge noise characteristics that govern the PL fluctuation dynamics. Within the framework of spectral noise analysis, the PL fluctuations are characterized by the noise spectral density $S(f)$ (see Supporting Information for details). In solid state systems, $S(f)$ is commonly modeled by a general power law $1/f^{\alpha}$ with a system-specific exponent α in the range 0.5–1.5[13,42−44] with $\alpha = 1$ being the limit of pure $1/f$-noise or pink noise.[45] For a more intuitive interpretation of the spectral fluctuations in the nanotube PL due to switching events of individual charge traps in the dielectric support, we decomposed the noise spectral density into contributions of random telegraph noise $S_t(f)$, pink noise $S_p(f)$, and frequency-independent white noise S_w as

$$S(f) = a \cdot S_t(f) + b \cdot S_p(f) + c \cdot S_w \quad (1)$$

with the respective relative weights a, b and c ranging between 0 and 1, and $a + b + c = 1$ (see the Supporting Information for the normalization of the individual noise components).

The first term quantifies the fraction of random telegraph noise (RTN) with a Lorentzian noise spectral density $S_t(f)$ (see Supporting Information for details) arising from a fluctuating charge trap in close CNT proximity. The CNT on hBN with the PL evolution and noise spectral density in the left panels of Figure 4a,b, respectively, is representative for the case where one dominant charge fluctuator causes discrete jumps between two distinct PL energies resulting in nearly pure RTN (the solid line in the left panel of Figure 4b shows the decomposition into noise components according to eq 1 with $a = 0.99$, $b = 0.00$, and $c = 0.01$). The central panels of Figure 4a,b show a CNT on hBN with a large $1/f$-noise component ($a = 0.74$, $b = 0.21$, and $c = 0.05$), and the right panels of Figure 4a,b are representative for CNTs on SiO_2 with a large white noise contribution (with $a = 0.64$, $b = 0.05$, and $c = 0.31$ for this specific tube). Whereas $1/f$-noise (pink dashed lines in Figure 4b) can be related to a superposition of multiple independent RTN sources,[46] very rapid fluctuations with a broad distribution of random amplitudes result in frequency independent white noise (gray dashed lines in Figure 4b).

We performed the decomposition of the noise spectral densities according to eq 1 for all CNTs of our study with PL time series recorded with a minimum of 1000 spectra at 1 s integration time. The resulting distribution of the noise compositions are summarized in the ternary plot of Figure 4c (blue and orange data correspond to CNTs on hBN and SiO_2, respectively). CNTs with vanishingly small spectral wandering were discarded from the analysis and are therefore not represented in the graph. For all other nanotubes, $S(f)$ was found to be dominated by the RTN component (similar to the three CNTs of Figure 4a,b) because of the dominant impact of the near-most charge fluctuator. Remarkably, the noise signatures of CNTs on hBN and SiO_2 again separate into two distinct classes: whereas nanotubes on hBN form a class with a varying $1/f$ noise contribution and a low white noise weight (<10%), the case of nanotubes on SiO_2 is just the opposite.

In order to interpret the spread in the data of Figure 4c, we performed Monte Carlo simulations to obtain $S(f)$ of the CNT PL originating from an exciton with a static dipole moment subjected to charge fluctuations in the dielectric support (see

DOI: 10.1021/acs.nanolett.8b00871
Nano Lett. 2018, 18, 4136−4140

Supporting Information for details on the model and the simulation results). In brief, we modeled a surface trap state as an elementary charge that together with its image charge in the dielectric substrate constitutes an electric dipole. Charge-capture and -release in a trap state at distance r results in a binary fluctuating dipolar vector field $\mathbf{F}$, which in turn gives rise to an energy shift $\Delta E_{PL} = \mathbf{p}\cdot\mathbf{F}$ of the nanotube PL via the first order Stark effect. We used $|\mathbf{p}| = 0.44$ eÅ for the static dipole moment of an exciton trapped at an oxygen side-wall defect[10] as an estimate for the dipole moments of localized excitons in our cryogenic CNTs.

First, we discuss the most obvious limit. A single-charge fluctuation site will lead to pure random telegraph noise. In the presence of a few sites, the near-most charge trap will dominate the spectral wandering because of the $1/r^2$ scaling of the PL energy shift with the distance to the charge, and the noise spectrum will be predominantly of RTN character as for the CNT in the left panels of Figure 4a,b. This statistically most common scenario explains why the fraction of RTN is large for all nanotubes observed on our sample (note the scale of the RTN weight in Figure 4c). A more general understanding of the origins of the two distinct classes of CNTs on hBN and SiO_2 was obtained from Monte Carlo simulations with a variable density of surface states (i.e., elementary charge traps) σ, their characteristic switching times τ, and minimum distance from the CNT r_{min} as input parameters.

The results of the simulations are included as gray-shaded data in Figure 4c. A rather stable dielectric environment with a low density of charge states and minute-long characteristic dwell times yields the expected large RTN components (black data points concentrated in the lower left corner of the ternary diagram in Figure 4b). Using the fluctuator areal density of $\sigma = 1 \times 10^{-12}$ cm^{-2} as characteristic for SiO_2,[47] the simulation results (light gray data) are in good agreement with the experimental data if typical fluctuation time scales in the range of 1−3 s are assumed in accord with the actual observation of switching events as in the upper and right panels of Figure 3a and Figure 4a, respectively. The large white noise component is introduced mainly by switching rates near and below the temporal resolution limit of 1 s in our experiment.

A region free of charge traps around the CNT exciton dipole yields the noise class of nanotubes on hBN with a sizable $1/f$-noise component. This limit (dark gray data in Figure 4b) is reproduced for distant ($r > 30$ nm) accumulations of charge traps with intermediate fluctuation times of ∼30 s and a factor of 10 higher spatial densities than on SiO_2. It reflects the case of an electrostatically calm substrate with a low charge trap density paired with distant chains of surface states. One possible realization of such a scenario is a CNT located close to a ridge of an extended atomically flat hBN terrace. At terrace ridges, both dangling bonds and accumulation of CVD catalyst particles can give rise to a collection of charge-state fluctuators with a high spatial density (this scenario is supported by complementary AFM and Kelvin probe microscopy, see Supporting Information). In fact, a posteriori inspection of luminescent CNTs with AFM has identified nanotubes in rocky regions of hBN flakes (right inset of Figure 4c) with the tendency to exhibit a higher $1/f$ noise component than tubes on extended terraces residing sufficiently far away form charge-fluctuating lines of disorder and thus exhibiting predominantly RTN in their spectral jitter (left inset of Figure 4c).

In conclusion, our study identifies luminescent CNTs as quantitative probes of charge fluctuations within their nearby surrounding. The complementary analysis of the Allan deviation and the noise spectral density of the temporal PL evolutions exhibited by individual CNTs on two different dielectric supports of this study suggests a 1 order of magnitude lower charge trap density on atomically flat hBN as compared to SiO_2, consistent with previous transport studies[31−34] and the improved spectral characteristics of two-dimensional semiconductors embedded in hBN.[35−38] Similar experiments can be performed to inspect the electrostatic stability of other dielectric substrates and environments using the PL of chemically doped CNTs[18−21] where defect-localized excitons exhibit dipole moments[9] of the order of 1 eÅ.[10] For such dipole moments, an elementary charge in a distance of 10 nm would result in a spectral PL shift of ∼1 meV, a value easily detected with standard spectroscopy. In contrast to alternative all-optical solid-state electrometers in the form of semiconductor quantum dots[11−14] and charged nitrogen vacancy centers in diamond,[15,16] defect-localized excitons in CNTs do not require a surrounding crystal matrix to maintain their photoactivity and thus can serve as sensing elements in scanning-probe electrometry with ultimate proximity to the object of interest.

■ ASSOCIATED CONTENT

Supporting Information

The Supporting Information is available free of charge on the ACS Publications website at DOI: 10.1021/acs.nanolett.8b00871.

Additional data as well as details on experimental methods and theoretical modeling (PDF)

■ AUTHOR INFORMATION

ORCID

Kenji Watanabe: 0000-0003-3701-8119
Adrian Bachtold: 0000-0002-6145-2479
Alexander Högele: 0000-0002-0178-9117

Notes

The authors declare no competing financial interest.

■ ACKNOWLEDGMENTS

This research was funded by the ERC Starting Grant 336749 and the ERC Advanced Grant 692876, the Foundation Cellex, the CERCA Programme, Severo Ochoa (SEV-2015-0522), the grant FIS2015-69831-P of MINECO, the Fondo Europeo de Desarrollo Regional (FEDER) and the German Excellence Initiative via the Nanosystems Initiative Munich (NIM). We also acknowledge financial support from the Center for NanoScience (CeNS) and LMUinnovativ. Growth of hexagonal boron nitride crystals was supported by the Elemental Strategy Initiative conducted by the MEXT, Japan and JSPS KAKENHI Grant Numbers JP15K21722 and JP25106006.

■ REFERENCES

(1) Heller, D. A.; Jin, H.; Martinez, B. M.; Patel, D.; Miller, B. M.; Yeung, T.-K.; Jena, P. V.; Höbartner, C.; Ha, T.; Silverman, S. K.; et al. *Nat. Nanotechnol.* **2009**, *4*, 114.

(2) Welsher, K.; Liu, Z.; Sherlock, S. P.; Robinson, J. T.; Chen, Z.; Daranciang, D.; Dai, H. *Nat. Nanotechnol.* **2009**, *4*, 773.

(3) Collins, P. G.; Bradley, K.; Ishigami, M.; Zettl, A. *Science* **2000**, *287*, 1801.

DOI: 10.1021/acs.nanolett.8b00871
Nano Lett. 2018, 18, 4136−4140

(4) Lefebvre, J.; Finnie, P.; Homma, Y. *Phys. Rev. B: Condens. Matter Mater. Phys.* **2004**, *70*, 045419.
(5) Leeuw, T. K.; Tsyboulski, D. A.; Nikolaev, P. N.; Bachilo, S. M.; Arepalli, S.; Weisman, R. B. *Nano Lett.* **2008**, *8*, 826.
(6) Withey, P. A.; Vemuru, V. S. M.; Bachilo, S. M.; Nagarajaiah, S.; Weisman, R. B. *Nano Lett.* **2012**, *12*, 3497.
(7) O'Connell, M. J.; Bachilo, S. M.; Huffman, C. B.; Moore, V. C.; Strano, M. S.; Haroz, E. H.; Rialon, K. L.; Boul, P. J.; Noon, W. H.; Kittrell, C.; et al. *Science* **2002**, *297*, 593.
(8) Bachilo, S. M.; Strano, M. S.; Kittrell, C.; Hauge, R. H.; Smalley, R. E.; Weisman, R. B. *Science (Washington, DC, U. S.)* **2002**, *298*, 2361.
(9) Hartmann, N. F.; Yalcin, S. E.; Adamska, L.; Háróz, E. H.; Ma, X.; Tretiak, S.; Htoon, H.; Doorn, S. K. *Nanoscale* **2015**, *7*, 20521.
(10) Glückert, J. T.; Adamska, L.; Schinner, W.; Hofmann, M. S.; Doorn, S. K.; Tretiak, S.; Högele, A. **2017** arXiv:1706.08347, accessed March 1, 2018.
(11) Vamivakas, A. N.; Zhao, Y.; Fält, S.; Badolato, A.; Taylor, J. M.; Atatüre, M. *Phys. Rev. Lett.* **2011**, *107*, 166802.
(12) Houel, J.; Kuhlmann, A. V.; Greuter, L.; Xue, F.; Poggio, M.; Gerardot, B. D.; Dalgarno, P. A.; Badolato, A.; Petroff, P. M.; Ludwig, A.; et al. *Phys. Rev. Lett.* **2012**, *108*, 107401.
(13) Kuhlmann, A. V.; Houel, J.; Ludwig, A.; Greuter, L.; Reuter, D.; Wieck, A. D.; Poggio, M.; Warburton, R. J. *Nat. Phys.* **2013**, *9*, 570.
(14) Hauck, M.; Seilmeier, F.; Beavan, S. E.; Badolato, A.; Petroff, P. M.; Högele, A. *Phys. Rev. B: Condens. Matter Mater. Phys.* **2014**, *90*, 235306.
(15) Dolde, F.; Fedder, H.; Doherty, M. W.; Nobauer, T.; Rempp, F.; Balasubramanian, G.; Wolf, T.; Reinhard, F.; Hollenberg, L. C. L.; Jelezko, F.; et al. *Nat. Phys.* **2011**, *7*, 459.
(16) Dolde, F.; Doherty, M. W.; Michl, J.; Jakobi, I.; Naydenov, B.; Pezzagna, S.; Meijer, J.; Neumann, P.; Jelezko, F.; Manson, N. B.; et al. *Phys. Rev. Lett.* **2014**, *112*, 097603.
(17) Hofmann, M. S.; Noé, J.; Kneer, A.; Crochet, J. J.; Högele, A. *Nano Lett.* **2016**, *16*, 2958.
(18) Ghosh, S.; Bachilo, S. M.; Simonette, R. A.; Beckingham, K. M.; Weisman, R. B. *Science* **2010**, *330*, 1656.
(19) Piao, Y.; Meany, B.; Powell, L. R.; Valley, N.; Kwon, H.; Schatz, G. C.; Wang, Y. *Nat. Chem.* **2013**, *5*, 840.
(20) Miyauchi, Y.; Iwamura, M.; Mouri, S.; Kawazoe, T.; Ohtsu, M.; Matsuda, K. *Nat. Photonics* **2013**, *7*, 715.
(21) Ma, X.; Hartmann, N. F.; Baldwin, J. K. S.; Doorn, S. K.; Htoon, H. *Nat. Nanotechnol.* **2015**, *10*, 671.
(22) Hofmann, M. S.; Glückert, J. T.; Noé, J.; Bourjau, C.; Dehmel, R.; Högele, A. *Nat. Nanotechnol.* **2013**, *8*, 502.
(23) Sarpkaya, I.; Zhang, Z.; Walden-Newman, W.; Wang, X.; Hone, J.; Wong, C. W.; Strauf, S. *Nat. Commun.* **2013**, *4*, 2152.
(24) Walden-Newman, W.; Sarpkaya, I.; Strauf, S. *Nano Lett.* **2012**, *12*, 1934.
(25) Fratini, S.; Guinea, F. *Phys. Rev. B: Condens. Matter Mater. Phys.* **2008**, *77*, 195415.
(26) Chen, J. H.; Jang, C.; Xiao, S.; Ishigami, M.; Fuhrer, M. S. *Nat. Nanotechnol.* **2008**, *3*, 206.
(27) Tans, S. J.; Verschueren, A. R. M.; Dekker, C. *Nature* **1998**, *393*, 49.
(28) Martel, R.; Schmidt, T.; Shea, H. R.; Hertel, T.; Avouris, P. *Appl. Phys. Lett.* **1998**, *73*, 2447.
(29) Lin, Y.-M.; Tsang, J. C.; Freitag, M.; Avouris, P. *Nanotechnology* **2007**, *18*, 295202.
(30) Star, A.; Gabriel, J.-C. P.; Bradley, K.; Grüner, G. *Nano Lett.* **2003**, *3*, 459.
(31) Dean, C. R.; Young, a. F.; Meric, I.; Lee, C.; Wang, L.; Sorgenfrei, S.; Watanabe, K.; Taniguchi, T.; Kim, P.; Shepard, K. L.; et al. *Nat. Nanotechnol.* **2010**, *5*, 722.
(32) Xue, J. M.; Sanchez-Yamagishi, J.; Bulmash, D.; Jacquod, P.; Deshpande, A.; Watanabe, K.; Taniguchi, T.; Jarillo-Herrero, P.; Leroy, B. J. *Nat. Mater.* **2011**, *10*, 282.
(33) Engels, S.; Epping, A.; Volk, C.; Korte, S.; Voigtländer, B.; Watanabe, K.; Taniguchi, T.; Trellenkamp, S.; Stampfer, C. *Appl. Phys. Lett.* **2013**, *103*, 073113.
(34) Baumgartner, A.; Abulizi, G.; Watanabe, K.; Taniguchi, T.; Gramich, J.; Schoenenberger, C. *Appl. Phys. Lett.* **2014**, *105*, 023111.
(35) Manca, M.; Glazov, M. M.; Robert, C.; Cadiz, F.; Taniguchi, T.; Watanabe, K.; Courtade, E.; Amand, T.; Renucci, P.; Marie, X.; et al. *Nat. Commun.* **2017**, *8*, 14927.
(36) Cadiz, F.; Courtade, E.; Robert, C.; Wang, G.; Shen, Y.; Cai, H.; Taniguchi, T.; Watanabe, K.; Carrere, H.; Lagarde, D.; et al. *Phys. Rev. X* **2017**, *7*, 021026.
(37) Ajayi, O. A.; Ardelean, J. V.; Shepard, G. D.; Wang, J.; Antony, A.; Taniguchi, T.; Watanabe, K.; Heinz, T. F.; Strauf, S.; Zhu, X.-Y.; et al. *2D Mater.* **2017**, *4*, 031011.
(38) Wierzbowski, J.; Klein, J.; Sigger, F.; Straubinger, C.; Kremser, M.; Taniguchi, T.; Watanabe, K.; Wurstbauer, U.; Holleitner, A. W.; Kaniber, M.; et al. *Sci. Rep.* **2017**, *7*, 12383.
(39) Allan, D. W. *IEEE Trans. Instrum. Meas.* **1987**, *36*, 646.
(40) Barnes, J. A.; Chi, A. R.; Cutler, L. S.; Healey, D. J.; Leeson, D. B.; McGunigal, T. E.; Mullen, J. A.; Smith, W. L.; Sydnor, R. L.; Vessot, R. F. C.; et al. *IEEE Trans. Instrum. Meas.* **1971**, *1001*, 105.
(41) Robinson, H.; Goldberg, B. *Phys. Rev. B: Condens. Matter Mater. Phys.* **2000**, *61*, R5086.
(42) Cleland, A. N.; Roukes, M. L. *Nature* **1998**, *392*, 160.
(43) Pelton, M.; Grier, D. G.; Guyot-Sionnest, P. *Appl. Phys. Lett.* **2004**, *85*, 819.
(44) Zhang, Y.; Moser, J.; Güttinger, J.; Bachtold, A.; Dykman, M. I. *Phys. Rev. Lett.* **2014**, *113*, 1.
(45) Hooge, F. N.; Kleinpenning, T. G. M.; Vandamme, L. K. J. *Rep. Prog. Phys.* **1981**, *44*, 479.
(46) McWhorter, A. L. *1/f noise and germanium surface properties*; Semicond. Surf. Phys., University of Pennsylvania Press: Philadelphia, PA, USA, 1957.
(47) Terman, L. *Solid-State Electron.* **1962**, *5*, 285.

DOI: 10.1021/acs.nanolett.8b00871
Nano Lett. 2018, 18, 4136−4140